Available online at www.sciencedirect.com
ScienceDirect
Journal of Catalysis 244 (2006) 230–237
JOURNAL OF CATALYSIS
www.elsevier.com/locate/jcat

# Exfoliated titanate, niobate and titanoniobate nanosheets as solid acid catalysts for the liquid-phase dehydration of D-xylose into furfural

Ana S. Dias [a], Sérgio Lima [a], Daniel Carriazo [b], Vicente Rives [b], Martyn Pillinger [a], Anabela A. Valente [a,*]

[a] *Department of Chemistry, CICECO, University of Aveiro, Campus de Santiago, 3810-193 Aveiro, Portugal*
[b] *Departamento de Química Inorgánica, Universidad de Salamanca, 37008 Salamanca, Spain*

Received 13 July 2006; revised 8 September 2006; accepted 12 September 2006

Available online 12 October 2006

**Abstract**

$HTiNbO_5$, $HTi_2NbO_7$, $HNb_3O_8$, $H_4Nb_6O_{17}$, and $H_2Ti_3O_7$ nanosheets obtained by exfoliation of protonated cation-exchangeable layered metal oxides were examined as solid acids for the cyclodehydration of xylose into furfural. The exfoliated-aggregated composites were characterized by powder X-ray diffraction, $N_2$ gas adsorption, and scanning electron microscopy, and the acid properties were measured by IR spectroscopy of adsorbed pyridine. In general, the materials had much higher catalytic activity than the nonexfoliated acid-exchanged layered materials. The initial catalytic activities of the exfoliated materials tended to increase with the total amount of acid sites (Brønsted + Lewis, B + L). Furfural yields of up to 55% were achieved after 4 h of reaction in a water–toluene solvent mixture under batch operation at 160 °C. Most of the materials could be recycled several times without loss of performance.


*Keywords:* Xylose; Furfural; Dehydration; Layered metal oxides; Exfoliation; Nanosheets; Solid acid

## 1. Introduction

Polysaccharides comprise the bulk of the world's annually renewable carbohydrate biomass. They compose a large number of monosaccharides, including glucose, fructose, and xylose. Xylose is obtained from annually harvested agricultural wastes and is transformed on an industrial scale into furfural by dehydration under acidic conditions [1]. Furfural is a versatile, renewable chemical with a wide industrial application profile both as a solvent and as a building block for the synthesis of various other chemicals, including tetrahydrofuran, agrochemicals, pharmaceuticals, fragrances, and furan-based resins [1–3]. Known industrial processes of furfural production use conventional mineral acids, such as sulfuric acid, as catalysts [1,4]. The cost and inefficiency of separating these catalysts from the products makes their recovery impractical, resulting in large amounts of acid waste that must be neutralized and disposed of. Other drawbacks of these processes include corrosion of the system and safety problems. Thus, the production of furfural is one of many industrial processes for which the demand for green chemistry and technology for sustainability [5,6] is stimulating the replacement of the "toxic liquid" acid catalysts by stable, recyclable, nontoxic solid acids [7].

Some recent progress has been made using inorganic or hybrid inorganic-organic solid acid catalysts for the dehydration of ketoses. D-xylose and D-fructose are catalytically converted to furfural and 5-hydroxymethyl-2-furaldehyde, respectively, by microporous faujasites and mordenites, with selectivities as high as 90% for ketose conversions below 30–40% [8]. The dehydration of fructose into 5-hydroxymethyl-2-furaldehyde over niobic acid ($Nb_2O_5{\cdot}nH_2O$) treated with phosphoric acid [9] and layered titanium phosphates [10] also has been studied; these materials exhibited better catalytic performance than previously reported heterogeneous catalysts. Recently, some of us reported that sulfonic acid-functionalized ordered mesoporous silicas are effective catalysts for the dehydration of D-xylose to furfural, using either dimethylsulfoxide (DMSO) or a water–toluene

* Corresponding author. Fax: +351 234 370084.
*E-mail address:* avalente@dq.ua.pt (A.A. Valente).

0021-9517/$ – see front matter 
doi:10.1016/j.jcat.2006.09.010

(WT) mixture as the solvent [11]. Heteropolyacids supported on mesoporous silicas were also tested for this reaction, giving furfural yields comparable with those obtained using $H_2SO_4$ under similar reaction conditions [12]. However, the supported heteropolyacids were partially leached into the aqueous phase during the catalytic reaction (in WT), which compromised the reusability of the catalysts. A microporous niobium silicate, designated as AM-11, was found to be more water-tolerant and can be reused in WT systems without loss of activity or selectivity between recycling runs [13].

Crystalline layered metal oxide cation exchangers, such as titanates and niobates, are potentially strong solid acids when in the $H^+$-form. However, the high charge density of the anionic sheets in these materials means that bulky substrate molecules cannot easily intercalate into the interlayer regions and react with $H^+$ ions. This problem has recently been addressed by exfoliating layered niobates and titanoniobates in aqueous solution to give colloidal single-crystal anionic nanosheets, which are then precipitated under acidic conditions to form aggregates of nanosheets [14–16]. The composites have much higher specific surface areas than the acid-exchanged layered precursors. Domen and co-workers found that whereas the formation and hydrolysis of ethyl acetate was not catalyzed by the nonexfoliated compounds $HTiNbO_5$, $HTi_2NbO_7$, and $HNb_3O_8$, the corresponding nanosheets functioned as strong solid acid catalysts for the reactions, rivaling or even beating niobic acid, which is a rare water-tolerant solid acid [17]. Herein we report on the catalytic performance of several transition-metal oxide nanosheets as solid acid catalysts for the cyclodehydration of xylose into furfural in aqueous phase. In situ IR spectroscopy of adsorbed pyridine is used for the first time to study the acid properties of these materials.

## 2. Experimental

### 2.1. Catalyst preparation

Layered alkali-metal titanate, niobates, and titanoniobates were prepared by conventional solid-state reactions in an alumina crucible, using $TiO_2$ (Sigma-Aldrich, 99.99%), $Nb_2O_5$ (Sigma-Aldrich, 99.99%), $Na_2CO_3$ (Chemikalien), $K_2CO_3$ (RPE, 99.9%), and $Cs_2CO_3$ (Sigma-Aldrich, 99.9%) as raw materials. $Na_2Ti_3O_7$ was prepared by heating a mixture of $Na_2CO_3$ and $TiO_2$ in a molar ratio of 1.1:3 at 800 °C for 18 h, and then for another 20 h at 800 °C after grinding [18]. For $K_4Nb_6O_{17}$ and $KNb_3O_8$, $K_2CO_3$ and $Nb_2O_5$ were mixed in molar ratios of 2.1:3 and 1.1:3, respectively, and heated at 1100 °C for 10 h for $K_4Nb_6O_{17}$ [19] and at 600 °C for 2 h and then at 900 °C for 3 h for $KNb_3O_8$ [20]. $KTiNbO_5$ and $CsTi_2NbO_7$ were prepared by heating mixtures of $K_2CO_3$ or $Cs_2CO_3$, $TiO_2$, and $Nb_2O_5$ in molar ratios of 1:2:1 and 1.1:4:1, respectively, at 1050 °C for 24 h for $KTiNbO_5$ [20], and at 750, 950, and 1050 °C for 12 h at each temperature for $CsTi_2NbO_7$ [21].

The obtained polycrystalline materials were converted to their protonated forms by immersion in 1 M HCl for $Na_2Ti_3O_7$ [22], 2 M HCl for $KTiNbO_5$ [23], 6 M HCl for $KNb_3O_8$ [24], and $CsTi_2NbO_7$ [25], and 6.5 M $HNO_3$ for $K_4Nb_6O_{17}$ [26]. The treatments were carried out at 60 °C for 1 week, with the acid solutions replaced with fresh solutions each day. Finally, the acid-exchanged materials were filtered, washed with distilled water, and dried overnight at 65 °C. Complete exchange of alkali ions was confirmed by powder X-ray diffraction (XRD) and energy-dispersive X-ray spectrometry (EDX).

Exfoliated sheets were obtained by adding 15 wt% tetra(*n*-butylammonium)hydroxide (TBAOH) solution to suspensions of the protonated compounds in distilled water (ca. 75 mL $g^{-1}$), as described previously [14–16,27]. The TBAOH solution was added until the pH reached 9.7, and the resultant mixtures were shaken for either 1 week ($eHTiNbO_5$) or 3 weeks ($eHNb_3O_8$, $eH_4Nb_6O_{17}$, and $eHTi_2NbO_7$). The insertion of voluminous and hydrophilic $TBA^+$ cations expands and hydrates the interlayer spaces, resulting in exfoliation of individual metal oxide sheets. Nonexfoliated particles were removed from the suspensions by centrifugation at 3000 rpm for 1 h, and the supernatant solutions containing the dispersed nanosheets were collected. The addition of an aqueous acid solution (20 mL, 1 M $HNO_3$ for $eHTiNbO_5$ and $eHTi_2NbO_7$, 0.1 M $HNO_3$ for $eHNb_3O_8$, and 0.5 M $H_2SO_4$ for $eH_4Nb_6O_{17}$) to 30 mL of a nanosheet solution resulted in immediate aggregation of the nanosheets as precipitates or gels. The aggregated samples were filtered, washed several times with distilled water, and dried at 65 °C. The precipitation of the $HTiNbO_5$ nanosheets was also achieved by addition of MgO fine particles (same weight as $HTiNbO_5$) to the nanosheet solution [27], giving a sample designated as $eHTiNbO_5$–MgO. The removal of the MgO particles was carried out by stirring the sample in 0.5 M $H_2SO_4$ overnight and finally washing with distilled water. Disappearance of $TBA^+$ in the final exfoliated samples was confirmed by elemental analysis for C and N. EDX confirmed that the sample $eHTiNbO_5$–MgO was free of MgO.

The exfoliation of $H_2Ti_3O_7$ was carried out using a different procedure than that described above [28]. A suspension of $H_2Ti_3O_7$ in an aqueous solution of methylamine (40 wt%) was sealed in a Teflon-lined stainless steel autoclave and stirred at 60 °C for 6 days. The resultant methylammonium/$Ti_3O_7$ intercalation compound was filtered and allowed to react in the autoclave with an aqueous solution of propylamine (50 vol%) at 60 °C for 6 days, giving a propylammonium/$Ti_3O_7$ intercalation compound. Excess amounts of the alkylammonium ions (20 and 40 mol of methylammonium and propylammonium per mol of $[Ti_3O_7]^{2-}$) were used for the reactions. A colloidal sol containing exfoliated titanate sheets was obtained by dispersing and swelling propylammonium/$Ti_3O_7$ in water (2 g $L^{-1}$), followed by sonication for 1 h and centrifugation at 3000 rpm for 30 min to remove precipitates (nonexfoliated materials). Aggregation of the nanosheets was done as described above using 1 M $HNO_3$.

### 2.2. Catalyst characterization

ICP-AES measurements were carried out at the Central Laboratory for Analysis, University of Aveiro (by E. Soares and co-workers), and microanalysis for C and N was car-

ried out on a Leco CHNS-932 instrument. Powder XRD data were collected at room temperature on a Philips X'pert diffractometer with a curved graphite monochromator (Cu$K_\alpha$ radiation), in a Bragg–Brentano para-focusing optics configuration (40 kV, 50 mA). Samples were step-scanned in 0.05° $2\theta$ steps with a counting time of 6 s per step. Brunauer–Emmett–Teller (BET) specific surface areas ($S_{BET}$) and specific total pore volumes ($V_t$) were estimated from $N_2$ adsorption isotherms measured at −196 °C, using a gravimetric adsorption apparatus equipped with a CI electronic MK2-M5 microbalance and an Edwards Barocel pressure sensor. The solids were outgassed at 150 °C before the measurements. SEM and EDX analyses were performed with a FEG-SEM Hitachi S4100 and a Rontec EDX, respectively. The pyridine adsorption experiments were carried out using a Perkin-Elmer 16PC apparatus and a specially designed Pyrex cell with $CaF_2$ windows, using self-supported sample discs (10–25 mg cm$^{-2}$). The samples were outgassed in situ at either 150 °C (eHTiNbO$_5$–MgO, e$H_4Nb_6O_{17}$, and e$HTi_2NbO_7$) or 400 °C (eHTiNbO$_5$ and e$HNb_3O_8$) for 2 h before adsorption of pyridine. A higher temperature had to be used for the last two samples to obtain a spectrum of reasonable quality. After degassing, pyridine was adsorbed at room temperature. The resultant samples were outgassed in situ at either 150 °C (eHTiNbO$_5$–MgO, e$H_4Nb_6O_{17}$, and e$HTi_2NbO_7$) or room temperature (eHTiNbO$_5$, and e$HNb_3O_8$) before the IR spectrum was recorded (at a resolution of 2 cm$^{-1}$).

### 2.3. Catalytic experiments

Batch catalytic experiments were performed under nitrogen in a tubular glass microreactor equipped with a valve for gas purging. In a typical procedure, D-xylose (30 mg), powdered catalyst (20 mg), and a solvent mixture (WT) comprising $H_2O$ (0.3 mL) and toluene (0.7 mL) were poured into the reactor. The reaction mixtures were heated with a thermostatically controlled oil bath and stirred magnetically at 500 rpm. The influence of the stirring rate on the initial reaction rate became negligible over 500 rpm. Zero time was considered the instant the microreactor was immersed in the oil bath.

The products present in the aqueous phase were analyzed using a Knauer K-1001 HPLC pump and a PL Hi-Plex H 300 × 7.7 mm i.d. ion-exchange column (Polymer Laboratories Ltd., UK), coupled to a Knauer 2300 differential refractive index detector (for xylose) and a Knauer 2600 UV detector (280 nm, for furfural). The mobile phase was 0.01 M $H_2SO_4$. Analysis conditions were a flow rate of 0.6 mL min$^{-1}$ and a column temperature of 65 °C. The furfural present in the organic phase was quantified using a Gilson 306 HPLC pump and a Spherisorb ODS S10 C18 column, coupled to a Gilson 118 UV/vis detector (280 nm). The mobile phase consisted of 30% v/v methanol in an aqueous solution with 10% methanol (flow rate, 0.7 mL min$^{-1}$). Authentic samples of D-xylose and furfural were used as standards, and calibration curves were used for quantification.

## 3. Results and discussion

### 3.1. Catalyst preparation and characterization

The exfoliation of acid-exchanged layered niobates and titanoniobates was carried out as described in the literature using aqueous tetra($n$-butylammonium)hydroxide. After centrifugation of the resultant colloids to remove small amounts of nonexfoliated particles, the exfoliated metal oxide nanosheets were precipitated by addition of acid solutions. The precipitation of $HTiNbO_5$ nanosheets was done by adding MgO fine particles to the nanosheet solution. This method was previously shown to improve the porosity and photocatalytic activity of a composite prepared from exfoliated $H^+/K_4Nb_6O_{17}$ [27]. $H_2Ti_3O_7$ exfoliated sheets were prepared by a different method than that used for the niobates and titanoniobates, involving sonication of a propylammonium/$H_2Ti_3O_7$ intercalation compound dispersed in water [28].

Fig. 1 shows the powder XRD patterns for the precipitated titanate, niobate, and titanoniobate nanosheets. The patterns for eHTiNbO$_5$, e$HTi_2NbO_7$, and e$H_4Nb_6O_{17}$ are in very good agreement with those reported by Domen and co-workers [14,15,29]. All six patterns have several features in common. The basal reflections—for example, (00$l$) for HTiNbO$_5$, (0$k$0) for $HTi_2NbO_7$, $HNb_3O_8$ and $H_4Nb_6O_{17}$, ($h$00) for $H_2Ti_3O_7$—are either broad and weak or not shown at all. For example, the XRD pattern of restacked HTiNbO$_5$ nanosheets has a weaker (002) diffraction peak (relative to the original nonexfoliated HTiNbO$_5$) and a complete absence of higher-order (00$l$) reflections. On the other hand, peaks in the $2\theta$ range of 20°–50°

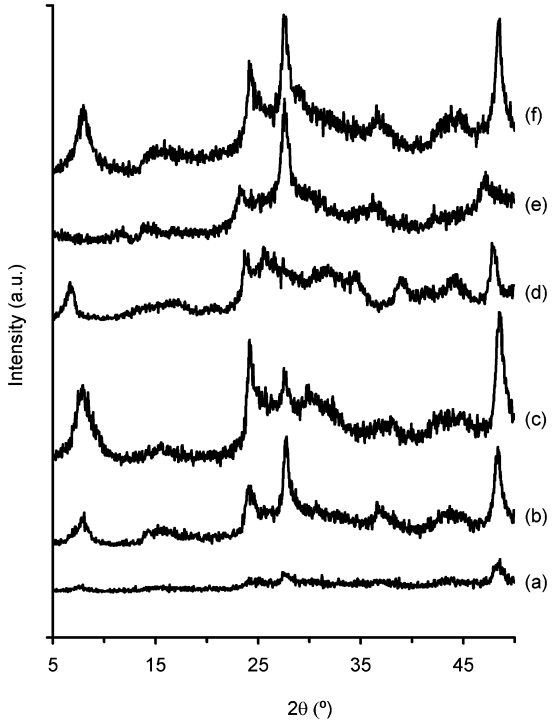


Fig. 1. Powder XRD patterns of aggregated metal oxide nanosheets: (a) eHTiNbO$_5$, (b) eHTiNbO$_5$–MgO, (c) e$HTi_2NbO_7$, (d) e$HNb_3O_8$, (e) e$H_4Nb_6O_{17}$, and (f) e$H_2Ti_3O_7$.

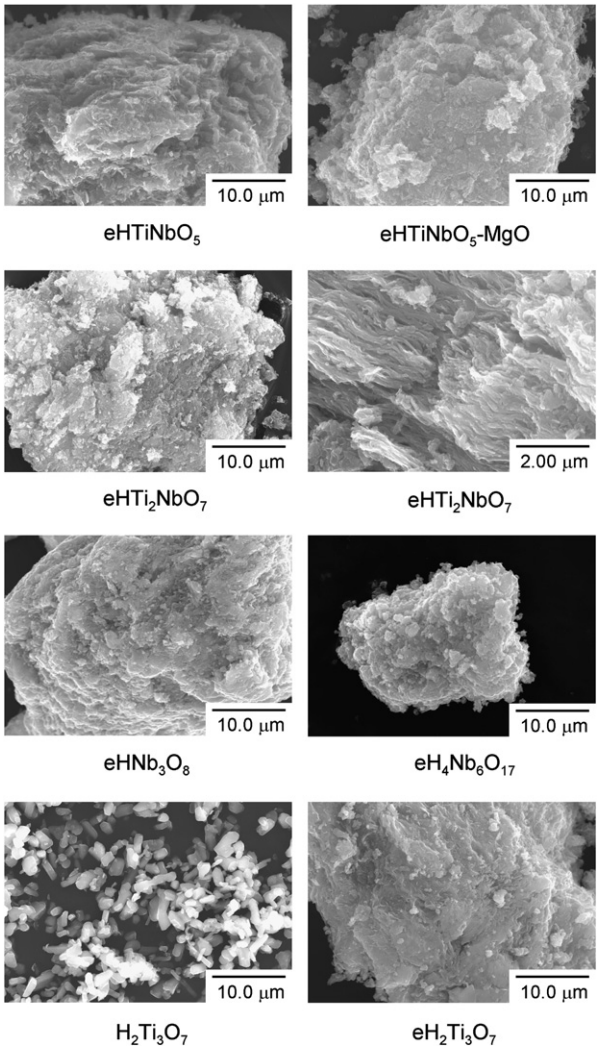


Fig. 2. SEM images of aggregated $HTiNbO_5$, $HTi_2NbO_7$, $HNb_3O_8$, $H_4Nb_6O_{17}$ and $H_2Ti_3O_7$ nanosheets ($eH_xTi_yNb_zO_n$), and the precursor non-exfoliated $H_2Ti_3O_7$.

corresponding to in-plane diffraction are preserved in the XRD patterns for all samples of precipitated nanosheets. This indicates that the order in the stacking of the transition metal oxide sheets is poor while the two-dimensional sheet structure remains [14,15,29]. Such a structure is also supported by the SEM images, which show aggregates composed of rather loosely and irregularly piled-up titanate, niobate, or titanoniobate sheets (Fig. 2). The samples are free of the tabular particles characteristic of the original nonexfoliated acid-exchanged materials (compare, e.g., $H_2Ti_3O_7$ and $eH_2Ti_3O_7$ in Fig. 2).

The BET specific surface areas ($S_{BET}$) of the precipitated nanosheets are given in Table 1. All of the layered acid-exchanged precursors have an $S_{BET} < 5\ m^2\,g^{-1}$, in agreement with literature data for these nonporous materials [15,16,24,27,29–31]. The aggregated nanosheets have a comparatively much higher $S_{BET}$, in the range of 40–136 $m^2\,g^{-1}$, indicating that the exfoliation-aggregation process developed micro/mesoporosity. Although the theoretical surface area of fully separated $HTiNbO_5$ nanosheets is about 330 $m^2\,g^{-1}$ [14], the measured surface area for $eHTiNbO_5$ is only 81 $m^2\,g^{-1}$. This

Table 1
Textural, acid and catalytic properties of the exfoliated-aggregated nanosheets

| Sample | $S_{BET}$[a] ($m^2\,g^{-1}$) | $V_p$[b] ($cm^3\,g^{-1}$) | Acid sites (mmol $g^{-1}$) | | | TOF[c] (mmol $g_{cat}^{-1}\,h^{-1}$) |
|---|---|---|---|---|---|---|
| | | | Brønsted | Lewis | Total | |
| $eH_4Nb_6O_{17}$ | 136 | 0.18 | 0.204 | 0.245 | 0.449 | 16.7 |
| $eHTiNbO_5$–MgO | 103 | 0.08 | 0.162 | 0.220 | 0.382 | 14.9 |
| $eHTi_2NbO_7$ | 88 | 0.08 | 0.085 | 0.226 | 0.311 | 13.8 |
| $eH_2Ti_3O_7$ | 57 | 0.03 | 0.007 | 0.135 | 0.142 | 10.9 |
| $eHTiNbO_5$ | 81 | 0.04 | 0.008 | 0.042 | 0.050 | 8.0 |
| $eHNb_3O_8$ | 40 | 0.03 | 0.007 | 0.039 | 0.046 | 4.7 |

[a] BET specific surface area.
[b] Pore volume calculated from $N_2$ adsorption at $p/p_0 \sim 0.97$.
[c] Turnover frequency calculated at 30 min reaction.

indicates that a fraction of the aggregated nanosheets was not accessible to the nitrogen molecules, probably due to intimate contact between nanosheets [14]. Precipitation of the $HTiNbO_5$ nanosheets by MgO fine particles instead of $HNO_3$ led to a higher specific surface area and total pore volume.

In the literature, the acid properties of some transition metal oxide nanosheets, obtained through the process of exfoliation of acid-exchanged samples followed by restacking, have been studied using color-indicator reagents, $NH_3$ temperature-programmed desorption ($NH_3$-TPD), and $^1H$ MAS NMR spectroscopy [14–16]. In the present work, the surface acidity of the samples was investigated for the first time (to the best of our knowledge) by in situ IR spectroscopy of adsorbed pyridine (Py-IR). Pyridine is widely used as a qualitative and quantitative probe to identify the concentration and nature of acid sites using the characteristic band of pyridinium ions at ca. 1540 $cm^{-1}$, as well as the band between 1440 and 1450 $cm^{-1}$ characteristic of pyridine bound coordinatively to Lewis acid sites [32–34]. The use of pyridine as a probe molecule (rather than $NH_3$) is arguably more appropriate for the present work, due to the fact that its molecular dimension approaches that of xylose.

For quantification, the molar absorption coefficients of the bands of adsorbed pyridine were set equal to those determined for zeolites [32]. The concentrations of Brønsted and Lewis acid sites determined in this way for the exfoliated and restacked samples are given in Table 1. After outgassing at 150 °C, all of the samples but $eHTiNbO_5$ and $eHNb_3O_8$ exhibit both Brønsted and Lewis acidity. No measurable surface acidity is observed for $eHTiNbO_5$ and $eHNb_3O_8$ when outgassing at 150 °C. However, the Py-IR spectra of these samples outgassed at room temperature shows the presence of some Brønsted and Lewis acidity. The poor results for the surface acidities of $eHTiNbO_5$ and $eHNb_3O_8$ may be due to the inaccessibility of the pyridine probe molecules to the acid sites (which probably also are inaccessible to xylose). For $eHTiNbO_5$–MgO, which has a higher specific surface area and total pore volume than $eHTiNbO_5$, the amount of acid sites measured by IR spectroscopy of adsorbed pyridine is correspondingly much greater. $NH_3$-TPD and $^1H$ MAS NMR studies reported in the literature for $eHTiNbO_5$, $eHTi_2NbO_7$, and $eHNb_3O_8$ reveal the presence of strong acidity (corresponding to at least 90% sul-

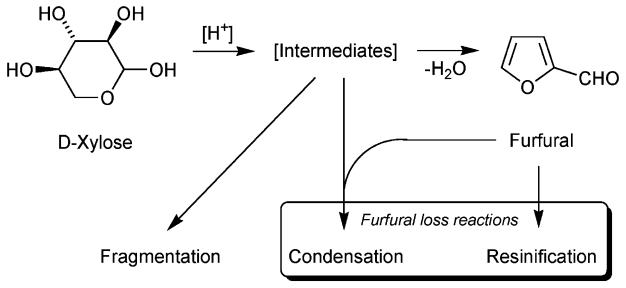


Scheme 1. Simplified reaction scheme of the dehydration of xylose to furfural and some side reactions.

furic acid), attributed to bridging hydroxyl groups of the type Ti(OH)Nb or Nb(OH)Nb ($H^+$ bonded to oxygen atoms shared by $Ti^{4+}$ and $Nb^{5+}$ or two $Nb^{5+}$) [14–16]. $^1$H MAS NMR and TGA allowed calculation of the density of these strong acid sites as 0.39 mmol $g^{-1}$ for $eHTiNbO_5$ and 0.36 mmol $g^{-1}$ for $eHTi_2NbO_7$ [14,15]. These values are significantly higher than the concentration of Brønsted acid sites measured by Py-IR, especially concerning $eHTiNbO_5$.

### 3.2. Catalytic cyclodehydration of xylose into furfural

The acid-exchanged layered and exfoliated titanate, niobates, and titanoniobates prepared in this work are active catalysts for the conversion of xylose into furfural, at 160 °C, in the aqueous phase, using toluene as a co-solvent for the extraction of the furfural formed during the reaction. It has previously been shown that the one-pot process of reaction and product separation leads to higher furfural yields than are achieved when only water is used as the solvent [11]. Similar results were recently reported for the fructose-to-hydroxymethylfurfural conversion [35]. The applied reaction conditions have been optimized to minimize the noncatalytic contribution relative to the catalytic contribution. Under these reaction conditions, the noncatalytic reaction at 30 min was negligible and gave 26% conversion and a 6% furfural yield after 6 h. Throughout this discussion, these results have not been corrected for this noncatalytic contribution.

The cyclodehydration of xylose involves a series of elementary steps in which the hydrogen ions transform hydroxyl groups of the pentose into $H_2O^+$ groups (the prerequisite for the liberation of water), resulting in the liberation of 3 water molecules per xylose molecule converted into furfural [1,4]. The byproducts formed in this reaction system result mainly from consecutive condensation reactions between furfural and intermediates of the xylose-to-furfural conversion (Scheme 1) [1].

The kinetic profiles of xylose conversion in the presence of the acid-exchanged niobate, titanate, and titanoniobates are shown in Fig. 3. For the nonexfoliated materials, the conversion versus time curves are all practically coincident (Fig. 3A). These materials are based on octahedral framework structures with $H^+$ ions located between the two-dimensional transition metal oxide anion sheets, and have a specific surface area (before and after catalysis) of $<5$ $m^2$ $g^{-1}$. The interlayer $H^+$ ions are probably not readily accessible to xylose, because intercalation of the reactant molecules will be inhibited by the high

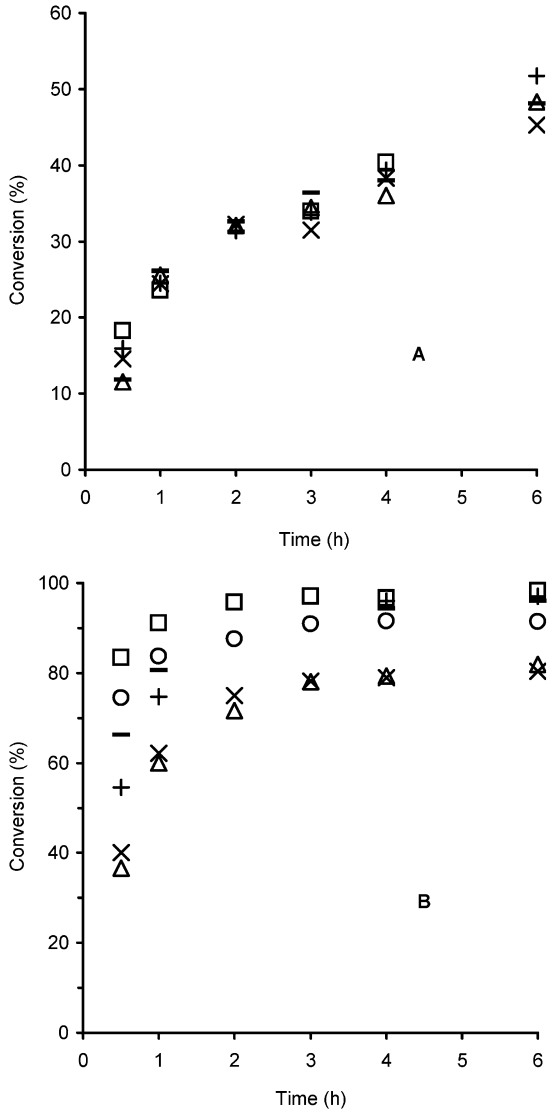


Fig. 3. Kinetic profiles of xylose conversion in the presence of the acid-exchanged layered (A) and exfoliated-aggregated nanosheet (B) catalysts: (e)$HTiNbO_5$ (×), e$HTiNbO_5$–MgO (○), (e)$HTi_2NbO_7$ (–), (e)$HNb_3O_8$ (△), (e)$H_4Nb_6O_{17}$ (□), and (e)$H_2Ti_3O_7$ (+).

charge density of the sheets. For $HTi_2NbO_7$ and $HTiNbO_5$, these layered materials were found to exhibit no catalytic activity for the esterification of acetic acid, cracking of cumene, dehydration of 2-propanol, and hydrolysis of ethyl acetate due to the narrow interlayer distance, whereas the exfoliated nanosheets function as effective strong solid acid catalysts [14,15]. Similar results have also been reported for $HNb_3O_8$ in esterification and hydrolysis reactions [16]. In the xylose-to-furfural conversion, the layered materials are not completely inactive, and catalytic turnover most likely occurs on active sites located on the exposed outer layers of crystals.

The exfoliated-aggregated materials generally have much higher catalytic activity than the layered materials for the cyclodehydration of xylose (Fig. 3B). Within 4 h of reaction, conversion reached 80–97% in the presence of the exfoliated catalysts, compared with a maximum of 40% for the layered materials. Xylose conversion increased with time for all cata-

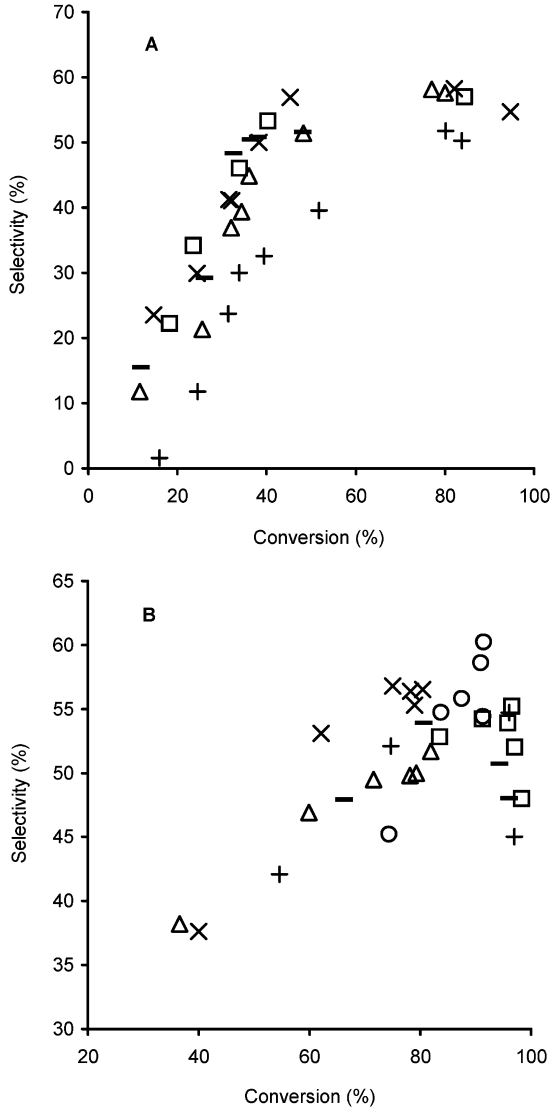


Fig. 4. Dependence of furfural selectivity on xylose conversion for the acid-exchanged layered (A) and exfoliated-aggregated nanosheet (B) catalysts: (e)$HTiNbO_5$ (×), e$HTiNbO_5$–MgO (○), (e)$HTi_2NbO_7$ (–), (e)$HNb_3O_8$ (△), (e)$H_4Nb_6O_{17}$ (□), and (e)$H_2Ti_3O_7$ (+).

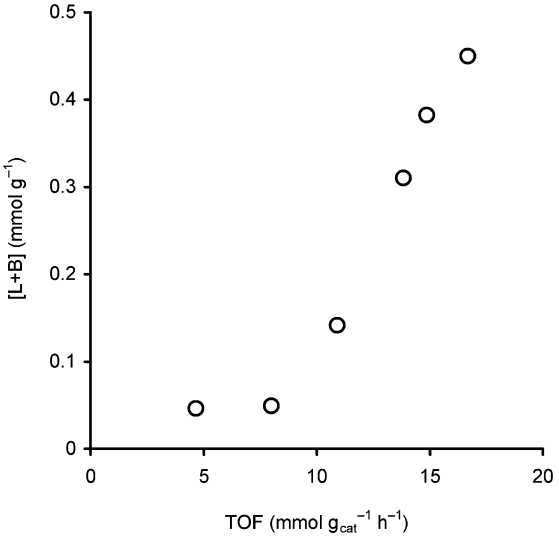


Fig. 5. Dependence of the initial catalytic activity (TOF) on the acid properties (B = Brønsted, L = Lewis) of the exfoliated-aggregated nanosheet solid acid catalysts.

lysts. In the case of e$HNb_3O_8$ and e$HTiNbO_5$, conversion after 3 h leveled off at about 80%, and selectivity also remained roughly constant (at 50 and 56%, respectively). This behavior may result from catalyst surface passivation due to strong adsorption of byproducts, as discussed below. On the other hand, it is also possible that a chemical equilibrium is attained through competitive adsorption effects; that is, unavoidable accumulation of products occurs under batch conditions.

The dependency of furfural selectivity on xylose conversion in the presence of the prepared catalysts is shown in Fig. 4. For the acid-exchanged layered materials, furfural selectivity increases with conversion, reaching 40–57% at 45–52% conversion, within 6 h of reaction (Fig. 4A). After 48 h, the maximum furfural selectivity was 58% at ca. 80% conversion. For the exfoliated materials, similar furfural yields were achieved at much lower residence times. For example, in the presence of e$HTiNbO_5$–MgO, furfural selectivity was 60% at 92% conversion (4 h), corresponding to a yield of 55% (Fig. 4B). In contrast to these results, the reaction was rather sluggish when carried out in the presence of $TiO_2$ or $Nb_2O_5{\cdot}nH_2O$, yielding only 10% or 12% furfural, respectively, at 4 h and 160 °C.

In general, selectivity tends to increase with xylose conversion, for conversions up to at least 60%. Similar results have been observed using homogeneous heteropolyacids or heterogeneous mesoporous solid acids as catalysts [11–13,36], which may be due to mechanistic factors. As mentioned above, the xylose-to-furfural conversion follows a complex reaction mechanism involving a series of elementary steps.

By increasing the reaction temperature from 160 to 180 °C, furfural yields of at least 55% could be achieved at even lower residence times (e.g., 57% at 2 h, for e$HTiNbO_5$–MgO; xylose conversion increased ca. 33%, whereas selectivity to furfural only increased by 3%).

The initial catalytic activities (TOF calculated after 30 min reaction) of the layered materials varied between 2.3 and 4.7 mmol $g_{cat}^{-1}$ $h^{-1}$. These values are lower than those observed for the exfoliated catalysts (Table 1), which follow the order e$H_4Nb_6O_{17}$ (16.7) > e$HTiNbO_5$–MgO (14.9) > e$HTi_2NbO_7$ (13.8) > e$H_2Ti_3O_7$ (10.9) > e$HTiNbO_5$ (8.0) > e$HNb_3O_8$ (4.7). The dehydration of carbohydrates can take place over Brønsted and Lewis acid sites [30,37]. Fig. 5 shows that the initial catalytic activity of the exfoliated materials tended to increase linearly with the total amount of acid sites (Brønsted plus Lewis, B + L) measured by IR spectroscopy of adsorbed pyridine under similar conditions. This trend was accompanied by an increase in specific surface area, with the exception of e$HTiNbO_5$ (Table 1). The most active catalyst (based on TOF) is e$H_4Nb_6O_{17}$, which also has the highest $S_{BET}$, $V_p$ and total amount of acid sites. For exfoliated e$HTiNbO_5$, the precipitation of the nanosheets by addition of MgO fine particles rather than 1 M $HNO_3$ gave aggregates with higher specific surface area, total pore volume, and total amount of acid sites, and a correspondingly higher initial catalytic activity. The beneficial

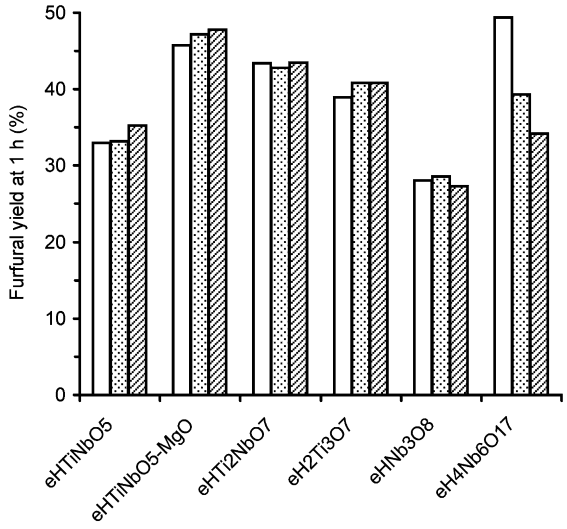


Fig. 6. Furfural yield obtained in recycling runs (run 1—white bar, run 2—dots, run 3—hashed) over the exfoliated-aggregated nanosheet solid acid catalysts.

effect of the MgO precipitation method on surface area and catalytic activity was also reported for $H^+/K_4Nb_6O_{17}$ used as a photocatalyst [27,30]. No clear relationship could be established between furfural yields at 1 or 4 h reaction and the acid properties of the exfoliated catalysts.

The catalytic stability of the nanosheets was investigated by recycling the recovered solids twice. After the reaction, the initially white solids became brownish. Before reuse, each catalyst was separated from the reaction mixture by centrifugation, washed thoroughly with methanol and acetone, and dried at 100 °C overnight. The solids retained a light-brown color after this procedure, suggesting the presence of organic matter strongly adsorbed on the catalyst surface. To remove coke, subsequent thermal treatment was applied to the recovered solids by heating at 350 °C (2° $min^{-1}$ heating rate), under air, for 3 h. The conditions of the thermal treatment were optimized (through elemental analysis for C and DSC) to efficiently remove coke. With the exception of $eH_4Nb_6O_{17}$, no significant loss of activity was observed between the first and third runs, and furfural yields remained roughly the same (Fig. 6). ICP analysis of the solutions after the reaction revealed no metal leaching. In the case of the hexaniobate $eH_4Nb_6O_{17}$, conversion decreased by a fraction of 0.13 from the first run to the third run and furfural yield dropped by ca. 15%. For this sample, the specific surface area decreased by 7% after reaction/regeneration, which may have decreased the number of effective acid sites somewhat.

## 4. Conclusion

The layered titanate, niobates, and titanoniobates and the corresponding exfoliated nanosheets are active and recyclable solid acid catalysts for the conversion of xylose into furfural at 160 °C under batch operating conditions, using water as solvent for xylose and toluene to extract furfural. The exfoliated nanosheets have higher specific surface area than the layered materials, leading to a higher amount of effective acid sites and consequently higher catalytic activity. After 4 h of reaction, xylose conversion of up to 92% and furfural yields of up to 55% were achieved with $eHTiNbO_5$–MgO. Increasing the reaction temperature to 180 °C led to similar results at much lower residence times. These results are much better than those obtained using sulfuric acid (25% furfural yield at 4 h and 160 °C). In general, the nanosheets are more active and somewhat more selective catalysts than the microporous AM-11 crystalline niobium silicates, which yielded more furfural than zeolites HY5 (the protonic form of Y-zeolite, with Si/Al = 5) and mordenite (Si/Al = 6), under similar reaction conditions [13]. Adjustment of the reaction conditions, such as temperature and residence time, together with reactor design could open up valuable perspectives in the application of transition metal oxide nanosheets to the conversion of saccharides into furan derivatives.

## Acknowledgments

This work was partly funded by the FCT, POCTI, and FEDER (project POCTI/QUI/56112/2004), Spanish Ministry for Science and Education (MAT2003-06605-C02-01) and ERDF. The authors wish to express their gratitude to Professor C.P. Neto for helpful discussions, Dr. F. Domingues (Department of Chemistry) for access to HPLC equipment, and M.F. Lucas for assistance with the HPLC analyses. A.S.D. and S.L. are grateful to the FCT for PhD and postdoctoral grants, respectively. D.C. thanks Universidad de Salamanca for a grant.

## References

[1] K.J. Zeitsch, The Chemistry and Technology of Furfural and Its Many By-Products, first ed., Sugar Series, vol. 13, Elsevier, Amsterdam, 2000.
[2] Y.L. Zhu, H.W. Xiang, Y.W. Li, H. Jiao, G.S. Wu, B. Zhong, G.Q. Guo, New J. Chem. 27 (2003) 208.
[3] A. Gandini, M.N. Belgacem, Prog. Polym. Sci. 22 (1997) 1203.
[4] B. Kamm, M. Kamm, P.R. Gruber, F. Kromus, in: B. Kamm, P.R. Gruber, M. Kamm (Eds.), Biorefineries—Industrial Processes and Products, vol. 1, Wiley–VCH, Weinheim, 2006.
[5] B. Horton, Nature 400 (1999) 797.
[6] P.T. Anastas, J.B. Zimmerman, Environ. Sci. Technol. 37 (2003) 94A.
[7] J.H. Clark, Acc. Chem. Res. 35 (2002) 791.
[8] C. Moreau, Agro Food Ind. Hi-Tech 13 (2002) 17.
[9] C. Carlini, M. Giuttari, A.M.R. Galletti, G. Sbrana, T. Armaroli, G. Busca, Appl. Catal. A Gen. 183 (1999) 295.
[10] F. Benvenuti, C. Carlini, P. Patrono, A.M.R. Galletti, G. Sbrana, M.A. Massucci, P. Galli, Appl. Catal. A Gen. 193 (2000) 147.
[11] A.S. Dias, M. Pillinger, A.A. Valente, J. Catal. 229 (2005) 414.
[12] A.S. Dias, M. Pillinger, A.A. Valente, Microporous Mesoporous Mater. 94 (2006) 214.
[13] A.S. Dias, S. Lima, P. Brandão, M. Pillinger, J. Rocha, A.A. Valente, Catal. Lett. 108 (2006) 179.
[14] A. Takagaki, M. Sugisawa, D. Lu, J.N. Kondo, M. Hara, K. Domen, S. Hayashi, J. Am. Chem. Soc. 125 (2003) 5479.
[15] A. Takagaki, T. Yoshida, D. Lu, J.N. Kondo, M. Hara, K. Domen, S. Hayashi, J. Phys. Chem. B 108 (2004) 11549.
[16] A. Takagaki, D. Lu, J.N. Kondo, M. Hara, S. Hayashi, K. Domen, Chem. Mater. 17 (2005) 2487.
[17] K. Tanabe, Catal. Today 78 (2003) 65.
[18] H. Izawa, S. Kikkawa, M. Koizumi, J. Phys. Chem. 86 (1982) 5023.
[19] T. Nakato, K. Kuroda, C. Kato, Chem. Mater. 4 (1992) 128.
[20] Y.I. Kim, S.J. Atherton, E.S. Brigham, T.E. Mallouk, J. Phys. Chem. 97 (1993) 11802.

[21] M. Hervieu, B. Raveau, J. Solid State Chem. 32 (1980) 161.
[22] T. Sasaki, F. Izumi, M. Watanabe, Chem. Mater. 8 (1996) 777.
[23] W. Hou, J. Ma, Q. Yan, X. Fu, J. Chem. Soc. Chem. Commun. (1993) 1144.
[24] W. Hou, B. Peng, Q. Yan, X. Fu, G. Shi, J. Chem. Soc. Chem. Commun. (1993) 253.
[25] H. Rebbah, M. Hervieu, B. Raveau, Mater. Res. Bull. 16 (1981) 149.
[26] M.A. Bizeto, D.L.A. de Faria, V.R.L. Constantino, J. Mater. Sci. 37 (2002) 265.
[27] R. Abe, K. Shinohara, A. Tanaka, M. Hara, J.N. Kondo, K. Domen, Chem. Mater. 9 (1997) 2179.
[28] N. Miyamoto, K. Kuroda, M. Ogawa, J. Mater. Chem. 14 (2004) 165.
[29] K. Domen, Y. Ebina, S. Ikeda, A. Tanaka, J.N. Kondo, M. Maruya, Catal. Today 28 (1996) 167.
[30] R. Abe, K. Shinohara, A. Tanaka, M. Hara, J.N. Kondo, K. Domen, J. Mater. Res. 13 (1998) 861.
[31] S. Papp, L. Kõrösi, V. Meynen, P. Cool, E.F. Vansant, I. Dékány, J. Solid State Chem. 178 (2005) 1614.
[32] C.A. Emeis, J. Catal. 141 (1993) 347.
[33] X. Li, K. Nagaoka, R. Olindo, J.A. Lercher, J. Catal. 238 (2006) 39.
[34] A. Corma, Chem. Rev. 95 (1995) 559.
[35] Y. Román-Leshkov, J.N. Chheda, J.A. Dumesic, Science 312 (2006) 1933.
[36] A.S. Dias, M. Pillinger, A.A. Valente, Appl. Catal. A Gen. 285 (2005) 126.
[37] T. Armaroli, G. Busca, C. Carlini, M. Giuttari, A.M.R. Galletti, G. Sbrana, J. Mol. Catal. A Chem. 151 (2000) 233.